Chapter 2
Laminar and Cellular Combustion of Hydrogenous Gaseous Mixtures

Keywords Additives • Flame propagation • Laminar flame

2.1 Measurement of Laminar Flame Velocity

Both stabilized (stationary) flame velocity and expanding (propagating) flame velocity can be measured in premixed gases (Fig. 2.1). The flame can be stabilized in various burners including opposed jet burners.

Schlieren photography of a spherical flame source and simultaneous pressure recording at constant volume conditions provide the best method for measuring propagating flame velocity. The most frequently used flame configurations are shown in Fig. 2.2. These geometrical configurations of the flame are preferable because their stretch effect can be controlled. A critical review of the methods for flame velocity measurements can be found in Andrews and Brandley's works [1, 2], and [3–8] as well.

Quantitative investigations of gaseous mixture combustion have been developed and upgraded since the first studies in the nineteenth century. The theoretical concepts of laminar flame velocity measurements have been developed by Gui and Michelson [9]. Michelson was the first who measured a flame velocity in a hydrogen + air mixture at atmospheric pressure and room temperature on the inner surface of a cone Bunsen flame [10]. Those unique and little known results were obtained for a wide range of hydrogen concentrations (from 15.3% to 74.6% of the mixture volume).

In the later work by Jahn [11] quoted in [6, 12] low hydrogen concentration mixtures were not considered (investigated hydrogen concentrations were 30% and higher), and maximum burning velocities (267 cm/s) were less than those measured by Michelson (281 cm/s). Kozachenko L.S. [13] replicated the Michelson measurements using a fantail burner; the results were close to those obtained by Michelson.

B.E. Gelfand et al., *Thermo-Gas Dynamics of Hydrogen Combustion and Explosion*,
Shock Wave and High Pressure Phenomena,
DOI 10.1007/978-3-642-25352-2_2,

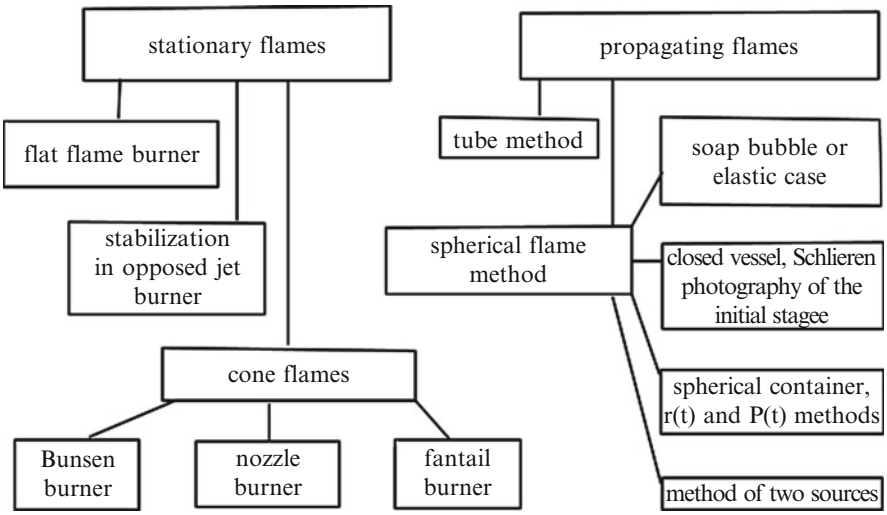

Fig. 2.1 Methods of laminar flame velocity measurements

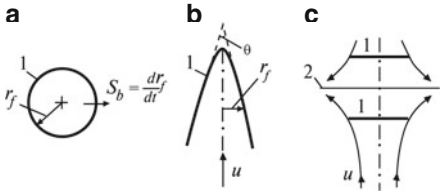

Fig. 2.2 The flame geometrical configurations providing controllable stretch effect: (**a**) spherical instable flame; (**b**) stationary cone flame; (**c**) stationary double flame in opposed jets. *1* – flame front; *2* – symmetry plane

Experimental data for hydrogen combustion obtained before 1956 have been discussed in [14]. In [15–19], both the theoretical premise and details of various experimental techniques for flame velocity measurements were considered.

A characteristic of a simple Bunsen burner is a parabolic profile of the unburned gas flow velocity. Moreover, the cone front area depends on a selected flame boundary (Schlieren, shadow or self-luminescence) [8]. Two ranges with strongly changing curvature (round vertex of the cone and the curves near the burner rim) are sources of inaccuracy [1, 12].

A nozzle burner has been used to obtain the uniform flow velocity profile. But it has been found in [15] that this velocity persists to be non-uniform due to the effect of the boundary layer on the burner rim; the use of larger diameter nozzles has been

Table 2.1 Laminar flame velocity S_u (cm/s) in hydrogen-air mixtures at the atmospheric pressure and the room temperature

Author	Year	Method	% H_2	S_u^{st}	S_u^{max}
Michelson	1889	Bunsen burner	15.3–74.6	217	281
Jahm	1934	Bunsen burner	30–75	187	267
Bartholome	1949	Nozzle burner	40–51.2	–	320
Kozachenko	1954	Fantail burner	20–70	233	287
Manton and Milliken	1956	Spherical flame	30–70	232	300
Fine	1956	Bunsen burner	28–62	193	304
Heimel	1956	Bunsen burner	28–57	206	297
Grummer	1959	Spherical flame	48–67.1	–	–
Senior	1961	Bunsen burner	17.4–33	200	–
Gunther and Janisch	1972	Nozzle burner	15–70	282	355
Andrews and Bradley	1973	Two sources method	10–70	–	336
Liu and MacFarlane	1983	Nozzle burner	20.6–64	–	356
Takahashi	1983	Nozzle burner	29.6–64	–	308
Wu and Law	1984	Nozzle burner	22.7–70	–	332
Wu and Law	1984	Nozzle burner	29.6–62.7	–	308
Iijima and Takeno	1986	Spherical flame	17.4–62.7	238	298
Dowdy, Smith, Taylor	1990	Spherical flame	9–68	213	286
Egolfopoulos, Law	1990	Counter-flow	9.7–38.6	209	
Koroll, Kumar, Bowles	1993	Two sources method	8–70	250	346
Koroll, Kumar, Bowles	1993	Nozzle burner	30–70	250	330
Vegelopopoulos and co-authors	1995	Counter-flow	9.5–18.8	–	–
Faeth and co-authors	1998	Spherical flame	15.9–62.7	210	247
Law and co-authors	2000	Spherical flame	15.9–627	190	282
Langmuir and co-authors	2003	Spherical flame	10–60	209	282
Huang and co-authors	2006	Spherical flame	20–38.7	224	–

recommended to minimize that effect. Comparison with the experimental data has shown that the flame velocities measured on nozzle burners were systematically higher than the values obtained in Bunsen burners.

Further, nozzle burners have been used in [16–18] for measurements in hydrogen-air flames and in [19, 20] for flames containing hydrogen, air and water steam.

Data collected in Table 2.1 and published in [10, 11, 13–33] illustrate the discrepancy in flame velocity values for hydrogen-air mixtures obtained by various measurement techniques at atmospheric pressure and room temperature.

A significant disadvantage of the burner method is the diffusion-thermal instability of the flame front in lean hydrogen-air mixtures (15% H_2 and less), which leads to non-uniformities of the flame concentration and temperature. Instead of a smooth cone, the flame in such mixtures takes the shape of a polyhedron with the alternation of luminous zones and zones where luminescence is not observed. The other proof of the non-uniformity is the cone vertex break. Experimental observations of the specific features referred to in lean hydrogen-air mixtures have been made in [34–36]. In [37] a theoretical description of the cone vertex break was presented.

Most of the early measurements were based on the concept of an infinitely thin flame front where the temperature is sharply changed from the initial value T_u to the burning temperature T_b, and the gas density falls from the unburned gas density ρ_u to the burn products density ρ_b at temperature of T_b. As a result of the thermal expansion, the visible flame velocity (the velocity relative to a motionless observer) S_b exceeds S_u. From the mass conservation law it follows that:

$$S_u = (\rho_b/\rho_u)S_b.$$

The value $\rho_u/\rho_b = \sigma$ - is the expansion ratio. The expansion ratio can be found experimentally by using photography of a flame propagating in a mixture filling a soap bubble or an elastic case. The expansion ratio can be computed by thermodynamic calculation of the combustion temperature and the equilibrium products composition at constant pressure. From the ideal gas state equation it follows that:

$$\sigma = (n_b T_b)/n_u T_u.$$

This method is applied at the initial stage of a spherical flame development, when the flame radius does not exceed one-half of a vessel radius. The measuring techniques for spherical laminar flame velocities have been considered in the literature [1, 3, 5, 21, 24, 27, 31–33, 38–43].

2.2 Results of Laminar Flame Velocity Measurements

Andrews and Bradley [1, 2] have analyzed the available measuring techniques and have proved the necessity to consider a flame front thickness when the spherical container method is used. They presented flame velocity data obtained in hydrogen-air mixtures contained in a closed space for both a single spherical flame source and for two flame sources moving toward each other.

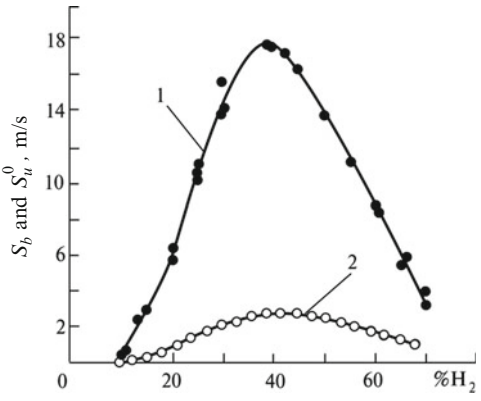

Fig. 2.3 The visible flame velocity measured by Andrews and Bradley [2] (1) and laminar flame velocity obtained by Dowdy and co-authors [27] (2) versus the percentage of hydrogen in H_2 + air mixtures. Temperature – 298 K, pressure – 0.1 MPa

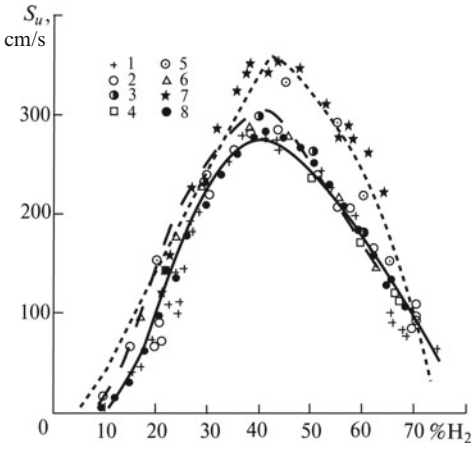

Fig. 2.4 The comparison of laminar flame velocities measured by various techniques in H_2 + air mixtures at atmospheric pressure and room temperature: *1* – Michelson [10]; *2* – Kozachenko [13]; *3* – Manton and Milliken [21]; *4* – Grumer [24]; *5* – Andrews and Bredley [2]; *6* – Iijima and Takeno [26]; *7* – Liu and MacFarlane [19]; *8* – Dowdy and co-authors [27]. The *short strokes* – Liu and MacFarlane correlated curvature. The *long strokes* – calculation performed by IChPh RAS (spherical flame). The *solid curves* – calculation performed by IChPh RAS (flat flame)

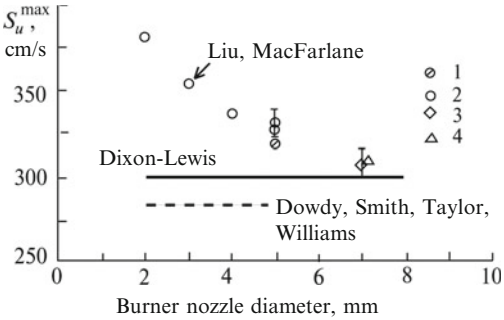

Fig. 2.5 The apparent laminar velocities in quick-burning H_2 + air mixtures in burners with different nozzle diameters. The measurements *1* – [15]; *2* – [44]; *3* – [45]; *4* – [46]. The Liu and MacFarlane measurements [19] signed with the *arrows*. The *dashed line* – measurements [27]. The *solid line* – calculations [38]

Figure 2.3 presents the values of visible velocity S_b of a single spherical source [2] and laminar flame velocity S_u^0 [27] for hydrogen-air mixtures. Later on, the double ignition method was used in [20] for measuring combustion velocities of both laminar and turbulent flames in lean hydrogen-air mixtures.

Figure 2.4 presents the laminar flame velocities measured by various techniques in H_2 + air mixtures. The results obtained by Liu and MacFarlane [19] noticeably differ from those obtained for a spherical flame and in a Bunsen burner, which is explained by the stretch effect. In [19] they used a small nozzle with a 3-mm diameter; it resulted in overrated combustion velocity values. Figure 2.5 presents

the data collection of maximum flame velocities measured for various diameter nozzles in H_2 + air mixtures. It is seen that the apparent velocity decreases with increasing nozzle diameter. All experimental data obtained for less-than 7-mm diameter nozzles are evidently higher than results obtained by the Dixon-Lewis numerical simulations [38] for a flat flame and from experimental data [27] extrapolated to an infinitely large flame radius on the basis of the Markstein phenomenological concept.

Data obtained for a smooth undisturbed flame by the spherical container method agree with the numerical simulation results of a spherical laminar flame propagation provided that an up-to-date detailed kinetic scheme with hydrogen oxidation and transport coefficients for describing multi-component diffusion of mass and heat are taken into account [27, 30, 43]. In some cases, when the agreement is not observed, it is necessary to analyze the arrangement of laminar flame velocity measurements.

A small number of experimental techniques is applicable for measuring a flame velocity in lean hydrogen mixtures. In such mixtures, effects requiring special attention to the arrangement of measurements of both laminar and turbulent flame velocities have been observed.

The value of S^0_u is important not only for simulating laminar and turbulent combustions and chemical kinetic problems, but also for designing various fuel burning devices. The value of S^0_u is a fundamental characteristic and denotes the velocity of a laminar stable adiabatic flat flame.

In practice, not all these conditions are met. It is the reason for a significant discrepancy in values of laminar flame velocity measured by various techniques and observed in some cases. For example, the difference in published values of the hydrogen-air flame combustion velocity in lean mixtures (15% H_2 and less) runs up to 2.5 times.

2.3 Development of Laminar Flame Velocity Measuring Techniques

Lately, efforts have been made toward the development of techniques to improve laminar and turbulent flame velocity measurements.

Flame velocity values depend on:

- Stretch effect,
- Nonadiabaticity,
- Finite combustion zone thickness,
- Flame instability.

Heat loss in burners has been quantified and has been taken into consideration. Application of opposed jet burners has allowed development of a method for determining a stretch-free flame velocity [28, 29]. The idea of this method is the determination of several S_u values at different stretch factors K and the further

extrapolation to $K = 0$. The necessity of extrapolation follows from the impossibility of stabilizing a flame at low K values.

It should be noted that the extrapolation method is complicated and time consuming. An absolutely different approach has been offered in [27, 47, 48]. It is based on a well-known technique for the investigation of a developing spherical flame using Schlieren photography. The idea of this method is to obtain a flame velocity correction relying on the Markstein assumption that such a velocity is a linear function of the flame curvature. The phenomenological ratio

$$S_b = S^0{}_b/\left(1 + b/r_f\right),$$

is used for the correction. After integration, this expression takes the form of an equation suitable for experimental data (flame radius r_f/time ratios) processing

$$r_f + b\ln r_f = S^0{}_b t + const.$$

Here $S^0{}_b$ is the visible flame velocity corrected to the stretch, b – experimental parameter. Parameter b takes into account two factors: a stretch and a flame thickness. If $S^0{}_b$, is known, than $S^0{}_u$ can be found by dividing the visible velocity by the expansion ratio $\sigma = \rho_u/\rho_b$. The ratio of unburned gas density ρ_u to the combustion product density ρ_b is found from the thermodynamic calculation.

Figure 2.6 presents expansion ratio values for H_2 + air combustion (solid curves) and H_2 + O_2 combustion (dashed curves) at several temperatures and at a fixed pressure of 0.1 MPa.

A somewhat different method has been used in [30, 49, 50]. In this method, firstly, a visible flame velocity $S_b = dr_f/dt$ is found by differentiating the experimental flame radius - time function and calculating the $S_u = S_b/\sigma$ value. A stretch correction has been performed by the linear extrapolation to zero flame curvature. Numerical experiments in [43] proved that the same value of $S^0{}_u$ can be obtained by use of either of the mentioned methods.

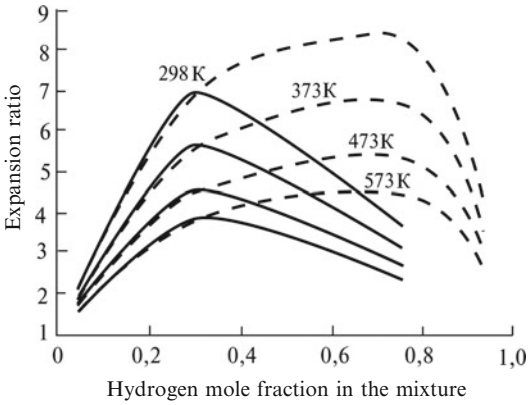

Fig. 2.6 The expansion ratio of hydrogen-air (the *solid curves*) and hydrogen-oxygen combustion products (the *dashed curves*) versus the composition and the initial temperature; $P = 0.1$ MPa

However, the numerical simulations have not used the experimental data, but the smooth calculation curves that have allowed finding the S^0_u value by linear extrapolation. In practice, the experimental dependencies do not correspond to the smooth curves and that method [49] proves to be less accurate than [51]. In some cases it is preferable to accept the flame velocity as a value found at maximum possible flame radius instead of an extrapolated value.

Apart from the flame velocity, the aforementioned methods of experimental ratios $r_f(t)$ processing can be applied to determining the Markstein length that is a measure of flame response to stretch, and can be positive or negative depending on the fuel composition. In recent years experimental data on the Markstein lengths for some hydrocarbon + air mixtures (including hydrogenous mixtures) have been obtained at atmospheric pressure, and a restricted number of the data points have been obtained at elevated pressure [30, 47–49, 52].

The possibility of determining a flame velocity corrected to the stretch in lean hydrogenous mixtures at higher than atmospheric pressure is still problematic. In particular, traditional methods of measurement result in a discrepancy between predicted and measured pressure characteristics of flame velocities at initial elevated pressure. For example, an expanding flame simulation in lean H_2 + air mixtures, when real kinetics and multi-component transport processes are taken into account, results in baric index values different from those obtained experimentally.

Measurement of laminar flame velocities is complicated in quick-burning $H_2 + O_2$ mixtures, and the data published are conflicting. It specifically relates to a high pressure combustion.

The amount of flame velocity experimental data for $H_2 + O_2$ mixtures is much less than for H_2 + air mixtures. Figure 2.7 presents a comparison between measured and calculated dependencies of the laminar velocity on mixture concentration over a wide range of the concentrations. Calculated flat flame velocities, those that take

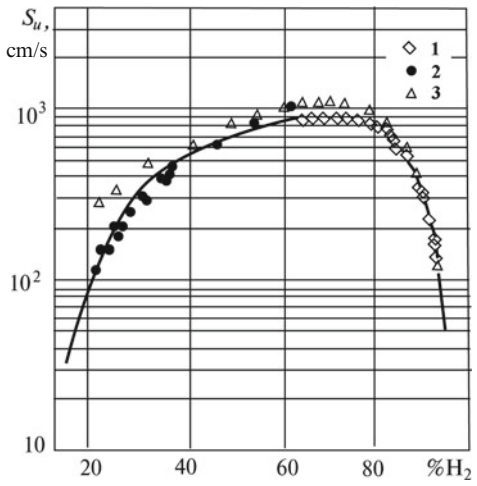

Fig. 2.7 The laminar flame velocities S_u in $H_2 + O_2$ mixtures at atmospheric pressure and 298 K temperature. The measured results [11] – *1* and [25] – *2* at Bunsen burner; [53] – *3* at nozzle burner. The *curve* – calculated data taking into account detailed kinetics

into account detailed kinetics and transport processes, are in better agreement with Jahn [11] and Senior [25] values measured in Bunsen burners, than those measured in nozzle burners [53].

Good experimental flame velocity data reproduction by numerical simulations allows using the simulation results when experimental data are not available.

2.4 Simulation of Flame Propagation

Currently, numerical simulations of flame propagation accounting for qualitative mixture compositions and multi-component transports have been widely performed. For example, calculation data of the laminar flame velocity in premixed H_2 + air mixtures at atmospheric pressure and room temperature have been published in [27, 38, 54–57].

Many investigators use a flat flame model for their calculations. The best known flat flame calculation algorithm PREMIX [58] has been developed by SANDIA. A characteristic feature of this simulation is that the laminar flame velocity is found as a stationary problem solution.

Another approach, introduced by Spalding [59], is a solution of the non-stationary one-dimensional problem and is usually called an iteration method.

The one-dimensional spherical flame developed from a small ignition source can be described by the mathematical model of [60] based on the mass, particles and energy conservation laws:

$$\partial\rho/\partial t + \nabla_r(\rho U) = 0, \tag{2.1}$$

$$\rho(\partial Y_i/\partial t) = \nabla_r(\rho D_{i,M}\partial Y_i/\partial r) - \rho U\partial Y_i/\partial r + W_i;\ \ i = 1, ..n, \tag{2.2}$$

$$W_i = \mu_i \sum_{j=1}^{k} v_{i,j}\, R_j,$$

$$\rho C_p(\partial T/\partial t) = \nabla_r(\Lambda\partial T/\partial r) - \rho U C_p \partial T/\partial r + \sum_{j=1}^{k}(-\Delta H_j)R_j, \tag{2.3}$$

$$\nabla_r A = 1/r^2 \cdot \partial(r^2 A)/\partial r, \qquad D_{i,M} = \frac{1 - Y_i}{\sum\limits_{j=1} x_j/D_{i,j}},$$

With the boundary conditions in the form of

$$\begin{aligned} (\partial T/\partial r)_{r=0} &= 0, & T_{r=R} &= T_0, \\ (\partial Y_i/\partial r)_{r=0} &= 0, & (\partial Y_i/\partial r)_{r=R} &= 0. \end{aligned} \tag{2.4}$$

Here: n and k are the number of components and reactions respectively, ρ, T, U are the gas density, temperature and velocity; μ_i, Y_i, x_i are the molecular weight, mass and volume fraction of particles i; C_p – specific heat capacity; $D_{i,j}$ – binary diffusion coefficient; $D_{i,M}$ – diffusion coefficient of particle i in the mixture; Λ – heat conductivity of non-reactive gases; ΔH_j – heat of elementary reaction j; $v_{i,j}$ – stoichiometric coefficients for particles i. The source term W_i depends on the reaction rate R_j.

In the case of freely propagating flames, vessel walls ($r = R$) are assumed to be located far from the flame front, which corresponds to the boundary conditions (2.4).

The model assumes that the burning process is initiated by the ignition source of radius R^*, duration - t^* and temperature $T^* > T_{\text{ad}}$, where T_{ad} – adiabatic flame temperature. The temperature condition (2.4) has the form:

$$t \leq t^* : T_{r \leq R^*} = const = T^*,$$

$$t > t^* : (\partial T / \partial r)_{r=0} = 0.$$

The reaction mechanism contains 26 elementary stages. The constants of velocity and efficiency of particles in tri-molecular reactions are taken following the recommendations given in [61–65].

Unlike the flat flame model [57–59], the approach offered in [60] allows investigation of the ignition process and further development of the spherical flame source. At small source radii the flame velocity reproduces the Lewis number effect. Figure 2.8 illustrates the spherical source development and allows comparison of radii predicted and measured using the Schlieren photography in an H_2 + air ($\phi = 0.26$) mixture.

2.5 Initial Temperature Effect on Laminar Flame Velocity

Change of the initial temperature in H_2 + air or H_2 + O_2 mixtures leads to a change in the flame velocity.

Figure 2.9 illustrates the temperature effect on the flame velocity in a stoichiometric H_2 + O_2 mixture at atmospheric pressure. The velocities measured from burners are shown by the solid circles [66], the calculated results [60] – by the curve. Most measurements in [66] were performed for lower temperatures, the range of high temperatures, which is of interest, have not been investigated. Measured results agree with the calculated data; however, the calculations were performed for a wider temperature range than the experimental measurements [66].

By using the flame velocity S_{u0}^* at temperature $T_0 = 298$ as a normalized value, Fig. 2.10 demonstrates the power law that can be applied to the approximation of the S_u dependence found for the temperature. The dashed parabolic curve shown in

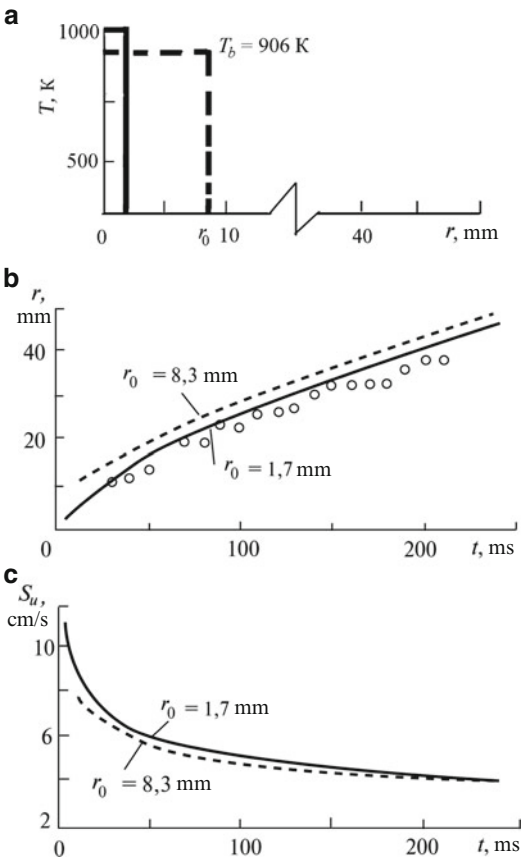

Fig. 2.8 The spherical flame radius and laminar flame velocity versus time for two ignition source sizes r_o: (**a**) initial temperature distribution; (**b**) the *curves*: calculated dependencies $r(t)$, the *open circles*: flame radii experimentally found using Schlieren photography; (**c**) flame velocity change with increasing radius

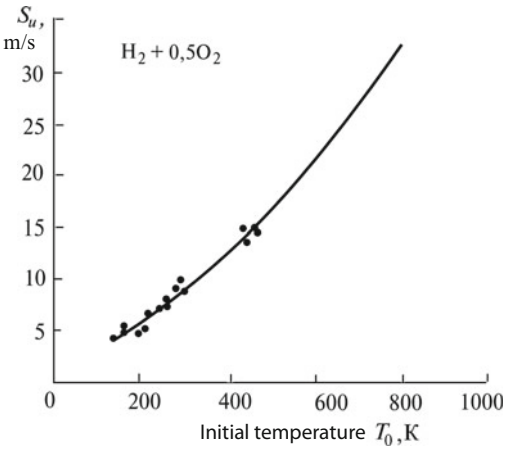

Fig. 2.9 The flame velocity versus temperature in a stoichiometric $H_2 + O_2$ mixture: the *solid circles* are experimental data [66]; the *curve* represents calculated data [60]

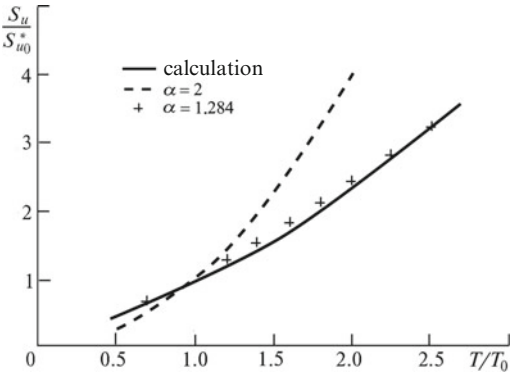

Fig. 2.10 The selection of the α exponent approximating the initial temperature dependence of the flame velocity in a $H_2 + 0.5O_2$ mixture

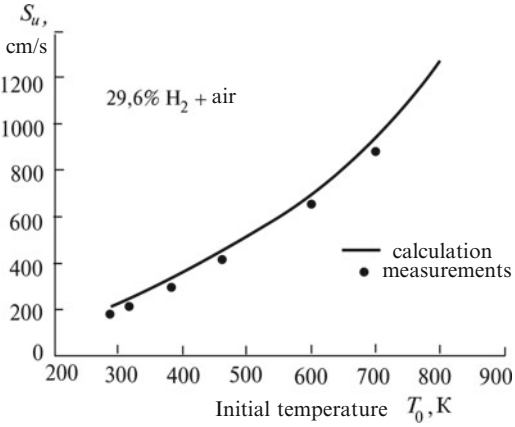

Fig. 2.11 The comparison of calculated and measured values of flame velocity versus temperature [23] for a stoichiometric H_2 + air mixture at atmospheric pressure

this figure is often used for hydrocarbons experimental data $S_u = S_{u0}{}^*(T/T_0)^\alpha$ approximation [6, 41]. Actual temperature dependence of the velocity is weaker for hydrogen, and for a stoichiometric $H_2 + O_2$ mixture it can be approximately described by the power function exponent $\alpha = 1.284$.

Laminar flame velocities have been measured in [23] for a stoichiometric H_2 + air mixture at various temperatures and atmospheric pressure. Figure 2.11 represents experimental and calculated [60] data. It is seen that the experimental data are in good agreement with the calculated ones in the range between 300 and 700 K.

Dependence of the calculated flame velocities [60] on the temperature in H_2 + air mixtures is presented in Fig. 2.12. The evident temperature dependence of the flame velocity was observed in a lean mixture containing 15% hydrogen.

Figure 2.13 illustrates other methods of laminar velocity prediction; it presents comparisons between measured results at 600 K temperature [23] and the calculated data. The calculations presented and the experiments prove that high flame velocities exist at elevated initial temperatures in H_2 + air mixtures. The obtained flame velocities are comparable with those observed in $H_2 + O_2$ mixtures at room temperature.

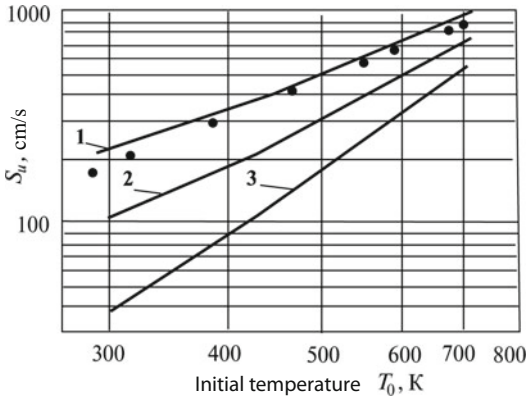

Fig. 2.12 The calculated flame velocities in H_2 + air mixtures at atmospheric pressure versus initial temperature: *1* – 29.6% H_2; *2* – 20% H_2; *3* – 15% H_2. The *solid circles* are measured results [23] in mixtures containing 29.6% H_2

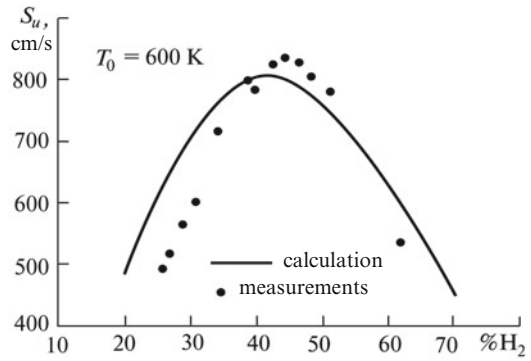

Fig. 2.13 The comparison of measured [23] and calculated [60] data on flame velocity S_u versus the hydrogen percentage in H_2 + air mixture at $T_0 = 600$ K

2.6 Pressure Effect on Laminar Flame Velocity

The pressure effect on a laminar flame velocity cannot always be reliably determined in experiments with hydrogen-containing mixtures. Contradictory conclusions for normal flame velocity dependence on pressure can be found in the literature. In technical applications, power functions for a flame velocity dependence approximation on temperature and pressure are used. Such power functions are called thermal and baric indexes respectively.

Often hydrogen mixtures are groundlessly assigned a thermal index equal to two. Experimental and calculated data presented show that this index changes depending on the mixture composition. The situation is more complicated with the baric index, because sometimes various measuring techniques result in opposite signs of the baric index. This leads to errors in the measured data extrapolation to uninvestigated pressure ranges.

One of the errors may be obtained by using the rule allegedly developed by Lewis [67] for hydrogen + air mixtures. The rule runs as follows: in mixtures with

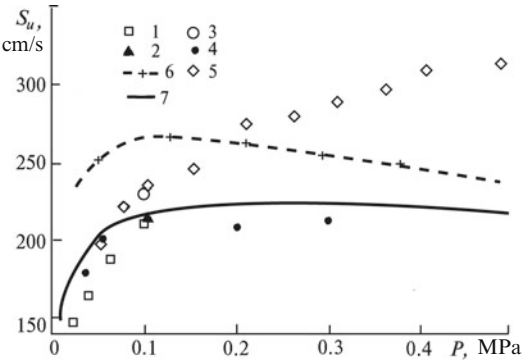

Fig. 2.14 The laminar flame velocity versus pressure in a stoichiometric H_2+air mixture at initial temperature 298 K, measured by various techniques: *1* – [22]; *2* – [27]; *3* – [41]; *4* – [30]; *5* – [26]; obtained by the numerical simulations: *6* – [55]; *7* – by the IChPh according to [60]

flame velocity exceeding 100 cm/s at atmospheric pressure, the predicted value grows with the pressure rise (positive baric index); on the contrary, in mixtures with 50 cm/s or less flame velocity, the laminar velocity falls with the pressure growth.

Authors [14, 67, 68] have presented the general dependence based on measurements in hydrocarbon fuels. The data collected disprove that empirical law, at least for mixtures containing hydrogen. Further results that compare the numerical simulation data with the conformable experimental results free from errors help to have a correct idea about flame behavior in hydrogen mixtures at various pressures.

At first, let us consider the laminar velocity - pressure dependence in a stoichiometric H_2 + air mixture at normal temperature 298 K. The solid curve in Fig. 2.14 illustrates calculated values of S_u^0 (for a flat flame) in the pressure range between 0.01 and 0.5 MPa. The laminar velocity - pressure dependence has a sloping maximum. All laminar velocity values are higher than 140 cm/s within this pressure interval. In the range up to 0.2 MPa the laminar flame velocity increases with the pressure, and after that it gradually falls.

A similar dependence for a stoichiometric H_2 + air mixture at temperature 300 K was obtained by numerical simulation considering the detailed kinetics [55] in the pressure range between 0.025 and 3 MPa. The laminar velocity calculated in [55] is higher than that obtained by the IChPh and presented in Fig. 2.14. The data at atmospheric pressure (268 cm/s) [55] are higher than the current experimental laminar velocity values (209–213 cm/s) measured in [27, 28, 30] (see Table. 2.1). The results obtained by the IChPh are in better agreement with the experimental results published in the literature excluding the measurements from [26] obtained in the higher pressure range.

The discrepancies can be explained by the fact that sometimes, for laminar velocity measurements done by the constant volume container method at elevated initial pressure, high-speed Schlieren photography was not used; the visible flame velocity was found either from the pressure records or from data on the front arrival time to a certain position (flame-ionization detectors, photodiodes). The experiments in [26] and [41] were performed in such a manner.

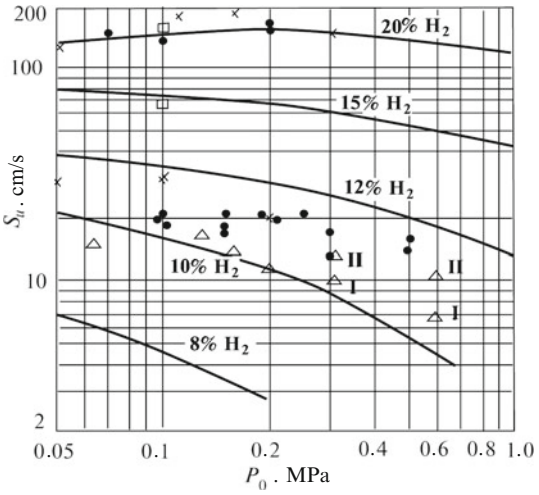

Fig. 2.15 The flame velocity - pressure dependencies in lean H_2 + air mixtures. The *curves* are calculated data. The measured results are: □ – according to [2], x – according to [69], • – $P(t)$, Δ – $r(t)$

When the flame is subjected to small-scale curvatures, which is typical for lean H_2 + air mixtures, an experimenter does not measure a normal velocity, but blindly measures some velocity depending on the level of the developing front. The front perturbation at an initial pressure of atmospheric or lower may be insufficient for a significant increase in the flame surface area. Therefore, even with the "blind" method of measurement in [26, 41], plausible results were obtained in the range between 0.05 and 0.1 MPa.

However, with the initial pressure growth the flame surface perturbations increase, which leads to discrepancies (see Fig. 2.15) between the calculated and the measured data on laminar flame velocities [26]. It can be said with confidence that the equations for the pressure index [26, 41] do not characterize a laminar flame in a H_2 + air mixture at elevated pressure.

Since lean mixtures are of interest, both from scientific and practical standpoints, IChPh RAS have analyzed the available experimental data on a laminar flame velocity and have performed experimental investigations and calculations in the lean range with 8% H_2 -20% H_2 in air [70]. The calculations were performed within the pressure range from 0.05 to 1 MPa. Figure 2.15 presents the calculated and measured data on the laminar flame velocity obtained by IChPh RAS in comparison with data from [2, 69].

The calculated dependencies, in the aforementioned pressure range with 8–15% H_2 concentration, illustrate the laminar flame velocity decrease with increasing pressure; a maximum close to 0.2 MPa was obtained, but only in a 20% H_2 mixture.

Notice the group of experimentally obtained points between the curves relevant to 10% and 12% H_2 mixtures. The solid circles denote results obtained by the "blind container" method where only $P(t)$ record processing was used for the flame velocity assessment. The empty triangles show results obtained in a similar

container by Schlieren photography of the initial stage of the flame development before the total pressure in the container has increased. In fact, it reduces the flame sphere radius to one-half of the container radius. The $P(t)$ record suitable for processing starts at the time when the Schlieren – registration $r(t)$ has finished.

If the flame sphere were smooth, the aforementioned measured results would be close to each other. This is true at atmospheric pressure. The discrepancies gradually increase with the initial pressure growth. The Schlieren photograph processing revealed a change in the slope of the $r(t)$ graph. It is caused by development of a front instability during the late stage of the flame sphere expansion. The laminar flame velocity assessed according to the second slope is denoted by II and the first slope – by I.

2.7 Mixture Composition Effect on Laminar Flame Velocity

The initial temperature T_0 and the pressure effect on the laminar flame velocity in lean H_2+air mixtures containing 10% H_2 (fuel excess coefficient $\phi = 0.26$) is presented in Fig. 2.16a, b. In Fig. 2.16a illustrates the pressure effect in the range

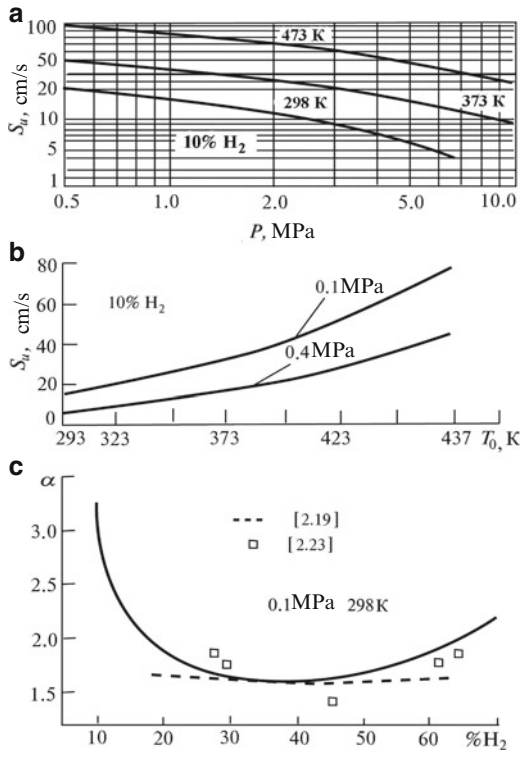

Fig. 2.16 The initial temperature and pressure effect on the flame velocity in lean H_2 + air mixtures (**a**, **b**). The change in the temperature index α as a the mixture composition according to the calculations (the *solid curve*) and the experimental results (the *dashed curve* and the *squares*) (**c**)

between 0.5 and 10 MPa. The solid curves relate to the laminar flame velocity calculated at initial temperatures of 298, 373 and 473 K.

The temperature effect is illustrated in Fig. 2.16b for 0.1 and 0.4 MPa pressure. It is seen that in the lean mixture the flame velocity falls with increasing pressure at constant temperature (negative baric index) and increases with temperature at constant pressure.

The temperature index α is given in Fig. 2.16c. for a wide range of H_2 concentrations in H_2+air mixtures. The temperature index of the laminar flame velocity has a minimum value in the range of H_2 content approximately between 30% and 45%; it grows in the lean and rich mixture ranges. The calculated temperature index data have been compared with the measured results of [19, 23]. For a complete description of the baric index values, $S_u(P)$ ratios, similar to those illustrated in Fig. 2.14 by the solid curve, can be differentiated to find the pressure range where the transition to the negative pressure index occurs.

Figure 2.17 presents values of $dS_u/d(P/P_0)$ for mixtures containing 29.6% H_2, 40% H_2, 60% H_2 and 70% H_2 that were calculated using the flat flame model [58] and the kinetic scheme applied in [60, 70]. The calculations have been performed for an initial temperature of 298 K. It is seen that the laminar flame velocity falls with increasing pressure throughout the entire range in the mixture containing 70% H_2. The feasible maximum flame velocity occurs near the lowest measured pressure.

Figure 2.18 demonstrates the laminar flame velocity - pressure dependence in the mixture containing 60% H_2 at 298 K. The solid curve denotes calculated velocities, the solid circles – experimental results [24] at lower and higher pressures than atmospheric. Measurements of both $P(t)$ and $r(t)$ records have been used in [24]. The discrepancies between velocity values obtained by two methods were insignificant (about 1–2 cm/s). The difference is explained by the fact that in the rich mixture containing 60% H_2 the flame sphere remained smooth even at pressures higher than atmospheric.

The data obtained by the spherical flame model are in close agreement with the aforementioned results. The model has been used for the laminar flame velocity calculation for the finite radius of the 3-cm sphere for 70% H_2 mixture at elevated

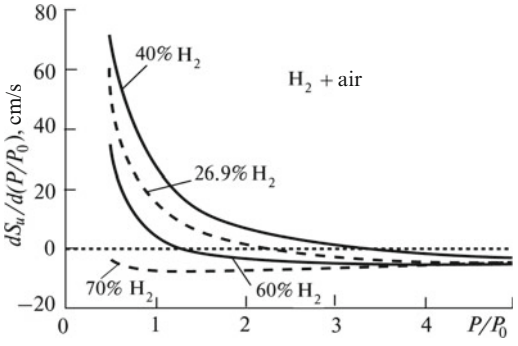

Fig. 2.17 The calculations of $dS_u/d(P/P_0)$ values for the H_2 + air mixtures at the initial temperature 298 K. $P_0 = 0.1$ MPa

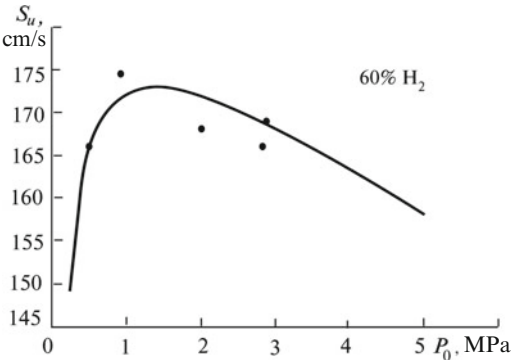

Fig. 2.18 The flame velocity change in the rich H_2 + air mixture (60% H_2) versus the initial pressure at 298 K temperature: the *curve* – calculations; the *solid circles* – measurements [24]

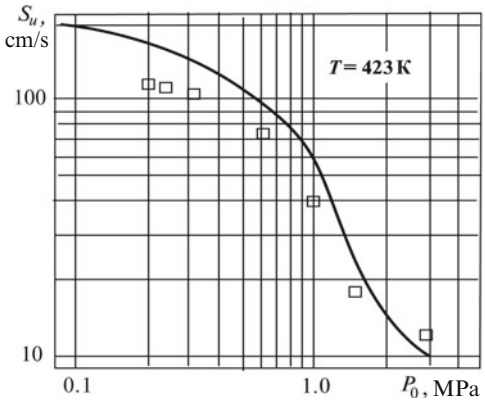

Fig. 2.19 The comparison of the numerical simulation data for a 70% H_2 + air mixture combustion at elevated temperature with the Babkin experimental results [71]: the *curve* – calculations; the *squares* – experiments

pressure and a temperature of 423 K. The temperature choice was based on the Babkin experimental data [71].

The solid curve in Fig. 2.19 illustrates the calculated laminar flame velocities and is compared with the experimental data denoted by the solid circles. Due to the elevated initial temperature (423 K) and atmospheric pressure, the flame velocity in the 70% H_2 mixture is higher than in the 60% H_2 mixture at room temperature (200 and 172 cm/s, respectively).

It has been noted in [71] and proved by numerical simulation data that the Lewis "rule" is not fulfilled in rich H_2 + air mixtures. Other cases when Lewis' "rule" is not correct for hydrogenous mixtures have been mentioned in [69].

Comparison of the calculated flame velocity data obtained by the kinetic simulation with the experimental results in H_2 + O_2 mixtures relative to the initial pressure effect on the flame velocity is of interest. Figure 2.20 demonstrates that the kinetic simulation predicts the laminar flame velocity growth with increasing pressure to approximately 2 MPa, after that the flame velocity falls. Similar results were obtained by the numerical calculation [54]. Such behavior of the flame velocity has not been proven experimentally. The work [72] presented the

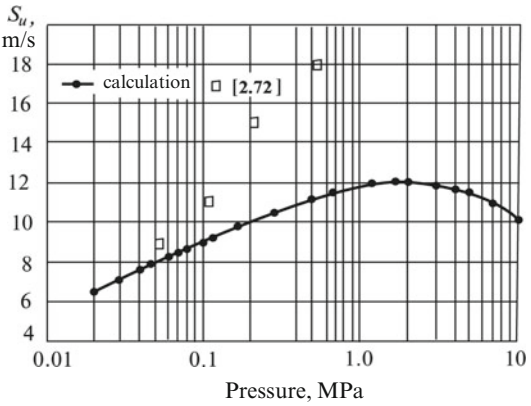

Fig. 2.20 The initial pressure effect on the flame velocity in $H_2 + O_2$ stoichiometric mixtures at 298 K. Comparison of the calculated and experimental data [72] obtained in the spherical container without Schlieren photography

measurements performed in the "blind" container within the 0.05–0.5 MPa pressure range, which gives evidence of the fractal nature of the flame front.

2.8 Effect of Noncombustible Gas Additives on Laminar Flame Velocity

Let us consider the effect of noncombustible additives, such as water steam, carbon dioxide or nitrogen on the laminar flame velocity along with combustion of binary fuel mixtures (H_2 + CO and H_2 + CH_4).

Noncombustible diluents reduce the laminar flame velocity due to a decrease in the flame temperature. Figure 2.21 illustrates the flame temperature T_b decrease and the decrease of the expansion ratio σ in two lean H_2 + air mixtures ($\phi = 0.39$ and $\phi = 0.26$) when water steam or carbon dioxide is added. As a diluent, CO_2 has a stronger effect because of its high heat capacity. If the water is added in the form of small drops, the picture is different, but here we are considering a gaseous diluent effect.

2.9 Carbon Dioxide Effect on Laminar Flame Velocity

Figure 2.22 illustrates the effect of a CO_2 diluent on the laminar flame velocity in a H_2+air mixture. Figure 2.22a shows a comparison between the measured and calculated laminar flame velocity values in three lean mixtures containing 14%, 10% and 8% H_2 before the dilution (ϕ = 0.39, 0.26 and 0.21 respectively). The relative reduction of the velocity S_u/S_{u_0}, where S_{u_0} denotes the flame velocity in the undiluted mixture, is presented in Fig. 2.22b. To reduce the velocity by half in the stoichiometric mixture (ϕ = 1) 20% of the CO_2 diluent is required, whereas in the lean mixture

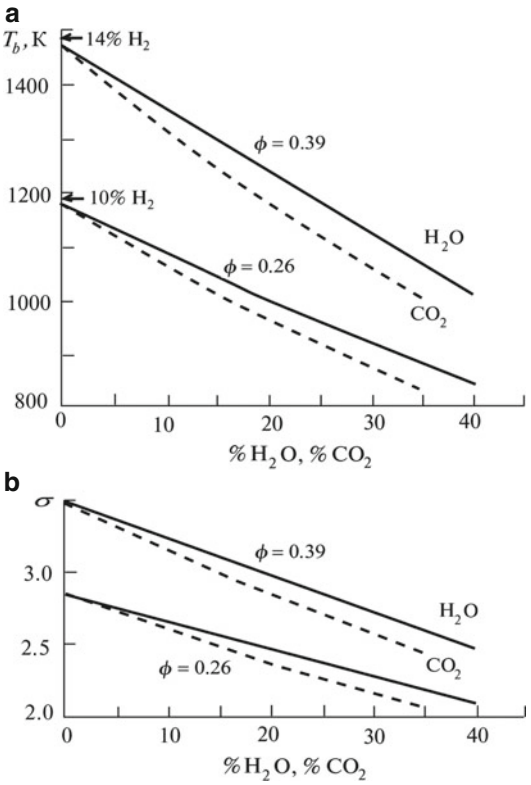

Fig. 2.21 The effect of water steam or CO_2 diluents on the flame temperature (**a**) and on the expansion ratio in lean H_2 + air mixtures (**b**). The *solid curve* – water steam diluent, the *dashed curve* – CO_2 diluent

($\phi = 0.39$) the velocity is cut in half at 10% CO_2 content. At the same CO_2 percentage the laminar flame velocity decrease is more evident in the lean mixtures.

The temperature and pressure effect is illustrated in Figs. 2.23 and 2.24. The curves represent the dependencies of laminar flame velocity on the temperature with a variable pressure parameter. It is seen that the velocity grows with the temperature increase at a fixed pressure, but it falls with increasing pressure at a fixed temperature value.

2.10 Water Steam Effect on Laminar Flame Velocity

The water steam effect on the laminar flame velocity is illustrated in Fig. 2.25. The steam content in the mixture is in the range between 12% and 43% at a temperature of 373 K and normal pressure. The relative content of H_2 in the H_2 + air mixture is plotted on the x-coordinate. The circles on the diagram denote the measured flame velocity results [44], the curves – the calculated data [73] from the kinetics simulation. The maximum values of the laminar flame velocities correspond to

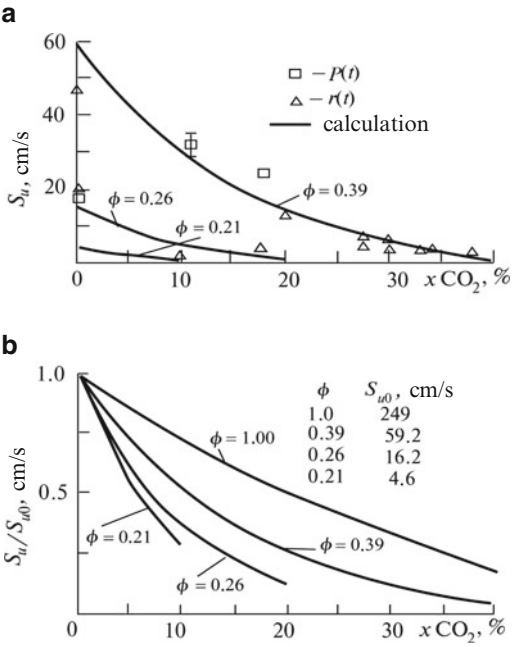

Fig. 2.22 The effect of a CO_2 additive on the flame velocity in H_2 + air mixtures at atmospheric pressure: (**a**) the measured and calculated flame velocities in the lean mixtures; (**b**) relative reduction of the flame velocity for mixture dilution with CO_2 at various fuel excess coefficient ϕ

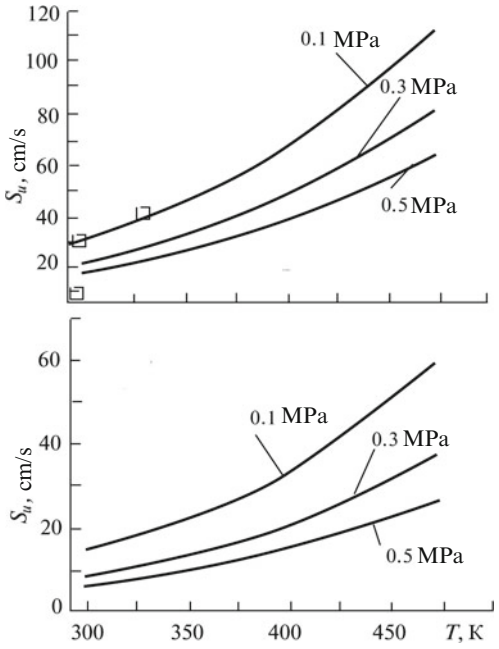

Fig. 2.23 The flame velocity S_u versus the temperature and the pressure in lean H_2 + air mixtures with CO_2 additive: the *curves* – calculated data; the *squares* – pressure/combustion time records processing in the spherical container; $\phi = 0.39$, (**a**) 10% CO_2; (**b**) 20% CO_2

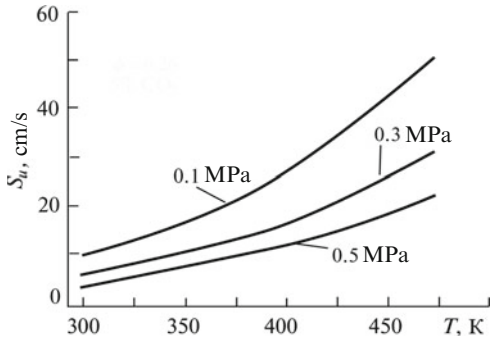

Fig. 2.24 The flame velocity S_u versus the temperature and the pressure in lean H_2 + air mixtures with CO_2 additive: $\phi = 0.26$, 5% CO_2

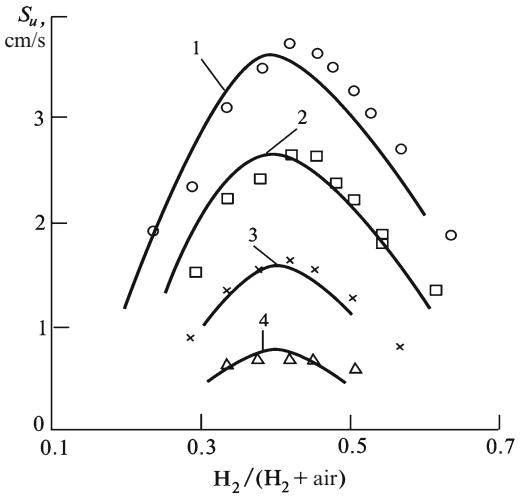

Fig. 2.25 The flame velocities in H_2 + air + H_2O (steam) mixtures at $T_0 = 373$ K and $P_0 = 0.1$ MPa: *1* – 12 vol.% H_2O; *2* – 22%; *3* – 33%; *4* – 43%. The *open circles*, *squares*, *triangles* – measured results [44], the *curves* – calculated data [73]

practically the same $H_2/(H_2 + air)$ ratio and is approximately equal to 0.4–0.45 and, in fact, close to the ratio in undiluted H_2 + air mixtures.

To verify the feasibility of the laminar flame velocity prediction in lean H_2 + air mixtures diluted with water steam at higher pressure, the calculation at 393 K temperature and 0.3 and 0.5 MPa pressures have been performed for the mixtures with $\phi = 0.26$ and $\phi = 0.39$.

Figure 2.26 presents the measured results (the open circles) and the calculated data (the curves) for the laminar flame velocity. The calculation and the experiments have been performed in the mixtures with various water steam content. In fact, the mixture with $\phi = 0.39$ cannot be diluted with more than 32% H_2O, and the mixture with over-fuel factor $\phi = 0.26$ cannot contain more than 12.5% H_2O.

The diagram in Fig. 2.27 illustrates the flame velocity decrease with the growth of the initial pressure in the $\phi = 0.39$ mixture diluted with water steam. The upper curve in Fig. 2.27 demonstrates the change in the mean baric index for the dry mixture; the two other curves denote the baric index change for the mixture diluted with water steam.

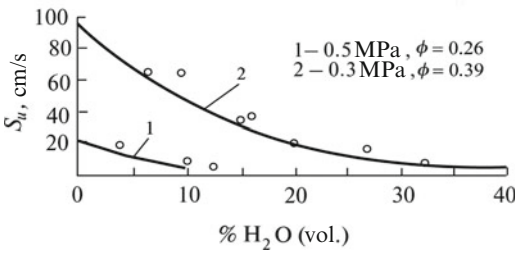

Fig. 2.26 The water steam effect on flame velocity in H_2 + air mixtures. The measured and calculated data on the flame velocity at 393 K temperature

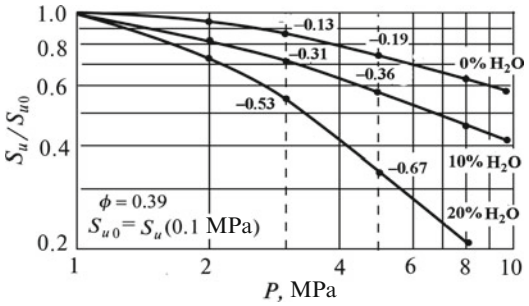

Fig. 2.27 The relative decrease in the flame velocity with the growth of the initial pressure in mixtures diluted with water steam. Figures on the curves indicate the pressure index β

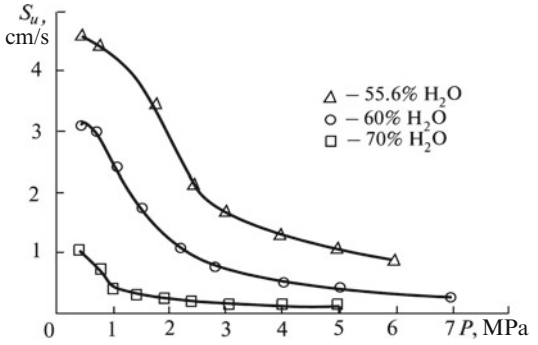

Fig. 2.28 The measured flame velocity in a stoichiometric mixture $H_2 + O_2 + H_2O$ (steam) versus the initial pressure, 473 K temperature and three different water steam concentrations

When the calculated and experimental data obtained at atmospheric pressure and higher (up to 0.5 MPa) are compared, it is apparent that the kinetic simulation method can be applied for combustion investigations in mixtures containing water steam. The kinetic simulation method can also be used for attempts to predict the behavior of H_2 + air + H_2O (steam) and H_2 + O_2 + H_2O (steam) mixtures in the range where experimental data are not available.

For substantial steam content and high pressure in H_2 + O_2 + H_2O (steam) mixtures, the quantitative discrepancy in predicted and realistic flame velocities dependence on pressure have been observed. The flame velocity measurements at 473 K and up to 7 MPa pressure in H_2 + O_2 + H_2O (steam) mixtures at the stoichiometric H_2/O_2 ratio have been published in [74] for the case when the mixture is diluted with steam (up to 70%).

Figure 2.28 presents the aforementioned data. The three curves for 55.6%, 60% and 70% steam content pass the pressure zone where S_u is rapidly decreasing. If the dependence $S_u = S_u(P, T)$ is written in the form

$$S_u(P,T) = S_{u0}(T/T_0)^{\alpha}(P/P_0)^{\beta},$$

where α and β are the flame velocity temperature and baric indexes respectively, then, in this zone $\beta = -1.5$ to -1 at 0.1 MPa. The sharp flame velocity fall with the pressure growth in $H_2 + O_2 + H_2O$ (steam) mixtures is proven by the calculations. But the measured velocity decreases more gradually with the pressure rise than is predicted by the calculation. Consideration of emission self-absorption by the water steam molecules decreases to some extent when the flame velocity falls at $P_0 = 2$–5 MPa, but it cannot explain the observed discrepancy.

A probable cause of the discrepancy between the calculated and measured S_u at the higher pressure is the change in the steam molecular structure such as formation of associates (dimers, trimers). Under this condition, the change in kinetic parameters of reactions with associated steam molecules can take place. The kinetic simulation has revealed that quantitative agreement between the experimental and calculated dependencies can be obtained with the assumption that the steam collision efficiency in a tri-molecular reaction $H_2 + O_2 + H_2O$ (steam) decreases with pressure growth. On the basis of [73] it can be assumed that at the high pressure the tri-molecular reaction effect on combustion of an oxy-hydrogen gas mixture with high water steam content is not as significant as could be expected based on the data obtained for low pressure.

It is of interest to compare the behaviors of $S_u(P)$ and $S_u(T)$ in the stoichiometric mixtures of $H_2 + O_2$ containing water steam and nitrogen. Experimental data [73] for the flame velocity pressure and temperature indexes for 0.2–0.8 MPa pressure and 373–473 K temperature are given in Table 2.2 along with values of S_u^0 at $P_0 = 0.14$–0.18 MPa and $T_0 = 373$ K.

Table 2.2 illustrates the change in sign of the baric index β from positive to negative when water steam is replaced by nitrogen. As this takes place, the temperature index α grows. In $H_2 + O_2 + H_2O$ (steam) flames with high velocities ($S_u > 1.5$ m/s) the baric index persists in being negative. This phenomenon has been observed in [75].

2.11 Laminar Flame Velocity in H_2 + CO + Air Mixture

Let us study a H_2 + CO mixture as a fuel. The flame velocities of rich H_2 + CO mixtures in air at atmospheric pressure and room temperature have been measured in [76]. Figure 2.29 presents the data obtained. Each curve in Fig. 2.29 corresponds to a constant CO/H_2 ratio, but the (H_2 + CO) fuel percentage in the air is changing. The upper curve represents pure H_2 fuel, and the lowest curve – CO with a small

Table 2.2 Mean experimental values α, β and S_u^0 (m/s) at combustion of stoichiometric mixtures $H_2 + O_2$ diluted with H_2O or N_2

vol.% H_2O, N_2	H_2O			N_2			P_0, MPa
	α	β	S_u^0	α	β	S_u^0	
55.6	2.23	−0.12	3.06	1.26[a]	0.26[a]	3.35[a]	0.18
60	2.65	−0.34	2.29	1.60	0.20	3.03	0.17
65	3.01	−0.46	1.22	1.82	0.13	2.50	0.155
70	3.28	−0.54	0.78	2.10	0.0	1.76	0.14

[a] Data reported by [41].

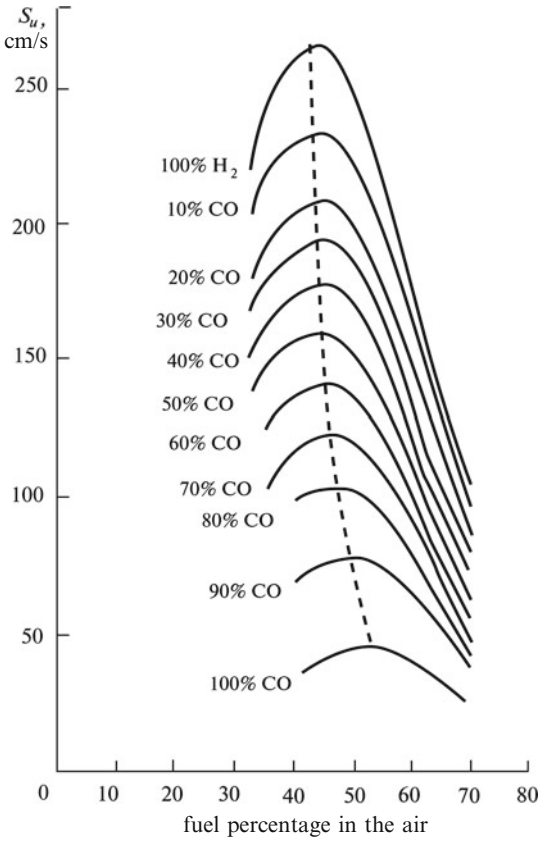

Fig. 2.29 The flame velocity at various (H_2 + CO) fuel concentration in air and at the percentage composition varying from 100% H_2 to 100% CO. The measurements have been performed in the burner [76] at atmospheric pressure and room temperature

content of water steam and H_2. Completely dry CO + air mixtures without any trace of hydrogenous components do not burn. The flame velocities have been measured in the burner, maximum S_u in the mixture free of CO is slightly lower than that obtained by modern methods of measurement.

The range of the stoichiometric and lean mixtures has been investigated in [77–79]. The authors in [77] have measured the flame velocity in spherical flames

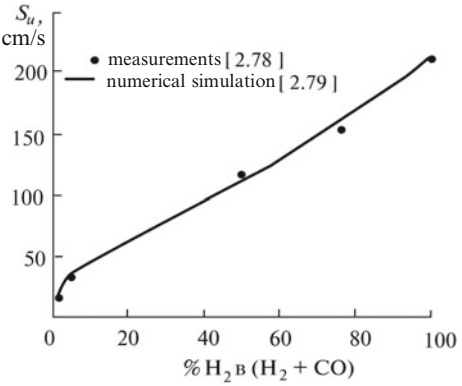

Fig. 2.30 The flame velocity in stoichiometric (H_2 + CO) fuel mixtures with air at 298 K and 0.1 MPa

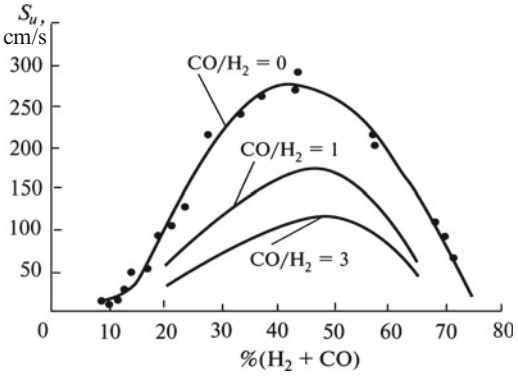

Fig. 2.31 The flame velocity in H_2 + CO + air mixtures where some of the H_2 is replaced by CO. The *upper curve* and the *solid circles* – measured results and their IChPh approximation by the least-squares method. The curves CO/H_2 = 1 and CO/H_2 = 3 – the measured data processing [79]. Initial conditions: atmospheric pressure, room temperature

of stoichiometric (H_2 + CO) + air mixtures, replacing some of the H_2 with CO. The dependence presented in Fig. 2.30 was obtained. The solid circles show the measured results and the line illustrates the numerical simulation data obtained in [78]. The applied method of flame velocity measurement is similar to the one described in [27, 48]. In [79] the flame velocities in H_2 + CO + air mixtures were obtained in the range between $\phi = 0.6$ and $\phi = 5$ and at pressures varying from 0.05 to 0.4 MPa.

Figure 2.31 illustrates the change in the laminar flame velocity in mixtures where some of the H_2 is replaced by CO. The CO/H_2 ratio is the varied parameter. The upper curve corresponds to a hydrogen–air mixture without CO. The solid circles show the flame velocities measured by Schlieren photographs of a spherical flame. The CO/H_2 = 1 and CO/H_2 = 3 curves were obtained by experimental data processing [79].

Additionally, in the range of the leanest mixtures containing H_2 + CO it was necessary to investigate combustion at both atmospheric and higher pressures. The

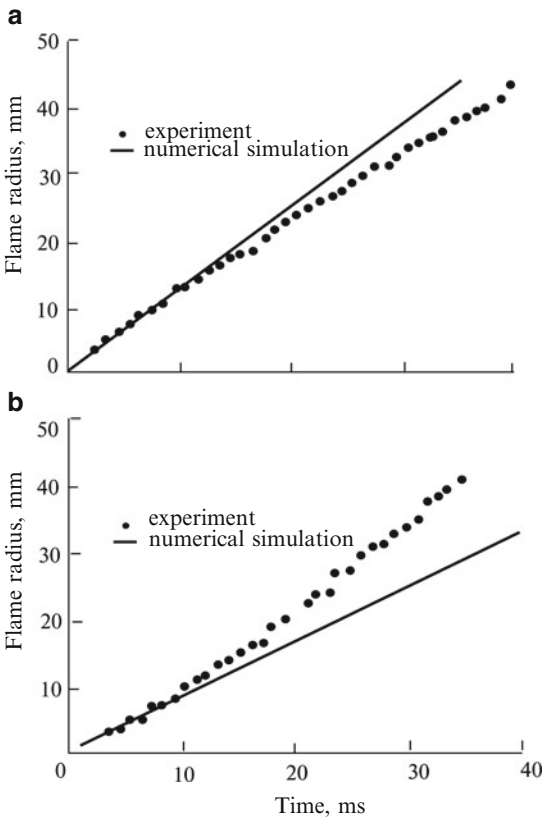

Fig. 2.32 The expansion of a spherical flame source in 15% (H_2 + CO) fuel+air mixture at $CO/H_2 = 1$. Temperature – 298 K, pressure – 0.1 MPa (**a**) and 0.3 MPa (**b**). Comparison of the numerical simulation data (the *curves*) with results obtained by Schlieren photography (the *solid circles*)

measurements of laminar and turbulent flame velocities were performed in [80–82]. Let us consider the flames that have not been subjected to artificial turbulence generation.

Let us study flame propagation in lean pre-mixed (H_2 + CO) fuel + air mixtures at equimolar H_2/CO ratio. The choice of fuel is justified by the known mechanism of CO oxidation in the presence of H_2 and by scanty amounts of experimental data on flame velocities in lean mixtures containing less than 20% (H_2 + CO). The measurements and the numerical simulation have been performed in the pressure range between 0.05 and 0.3 MPa at a fixed initial temperature 298 K. The premixed air mixtures with a fuel percentage from 10% to 20% (by vol.) have been investigated. The experiments were performed in a 3.8 L container with a center spark ignition. For the simulation, the spherical flame surface was assumed to be smooth. Thermal diffusion and convective motion were not considered.

Figure 2.32a, b presents the radius of the expanding flame source in relation to the time. Data were obtained by Schlieren photography and by numerical simulation.

The aforementioned data illustrate the behavior of a system containing two types of fuel, H_2 and CO, at molar ratio $CO/H_2 = 1$ and the total fuel concentration (H_2 + CO) equal to 15%. At 0.1 MPa pressure, a flame ball initially expands as is predicted by the detailed kinetic model. When the flame radius reaches 15 mm, the evident deceleration

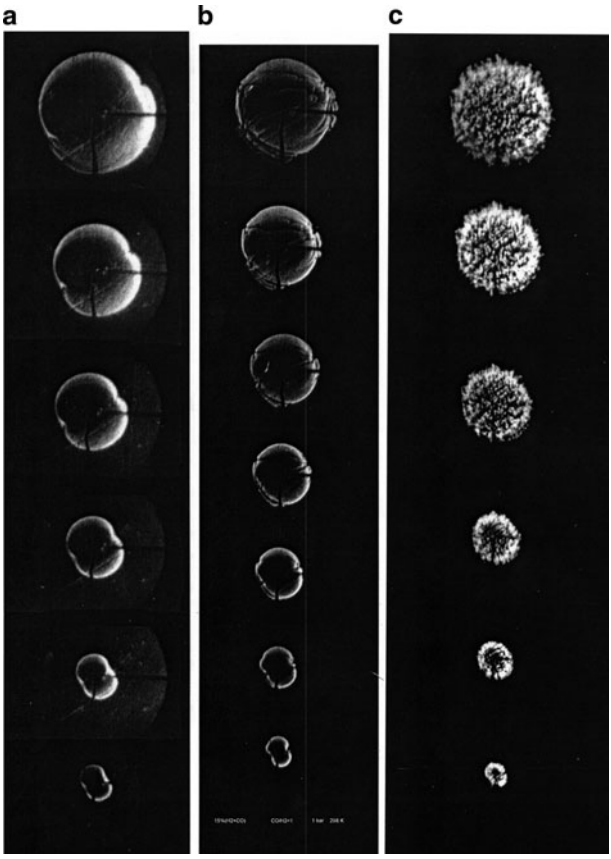

Fig. 2.33 Schlieren photography of the spherical flame source expansion in an air mixture with 15% (H_2 + CO) at CO/H_2 = 1 at 0.05 MPa (**a**); 0.1 MPa (**b**); 0.3 MPa (**c**). The *upper* photos correspond to 35–40 ms time from the ignition

followed by an acceleration that changes to a deceleration and vice-versa have been recorded. The peculiarities observed are not bound with the accuracy of the flame photos processing. Similar "pulsations" have been recorded in repeated experiments. But, in H_2 + air mixtures without CO additive, such a pulsing behavior was not observed.

Figure 2.33 presents photos testifying to the smooth flame front in CO + H_2 + air mixtures at lower than atmospheric pressure (0.05 MPa), the numerical simulation data agree with the experimental results up to 35 mm radius. Such measured results can be used for determining the laminar flame velocity. At 0.3 MPa pressure the flame surface is rough and the comparison with the simulation data allows finding the degree of front radius growth and the efficient flame velocity.

The obtained Schlieren photos show that the flame front changes with the pressure growth. At atmospheric pressure the flame in the mixture containing 15% (H_2 + CO) preserves its smoothness and no cells are evident, but at 0.2 and 0.3 MPa pressure the

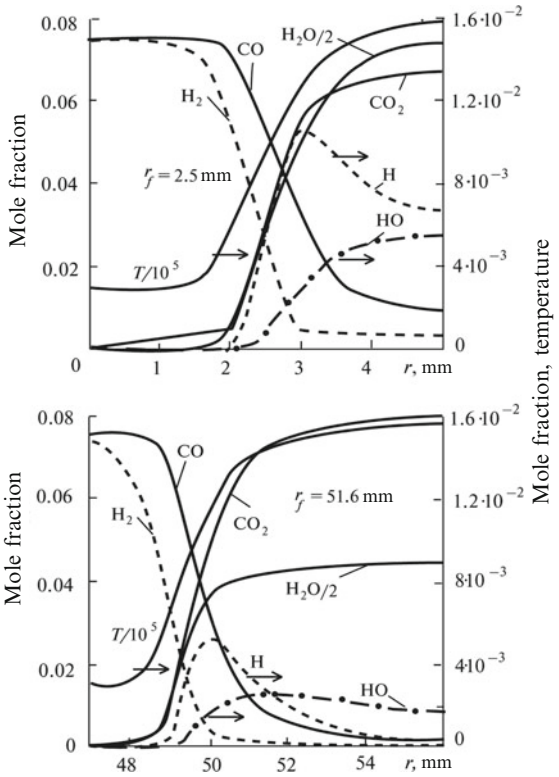

Fig. 2.34 The concentration profiles in the fuel+air mixture (H_2 + CO) ($CO/H_2 = 1$) at two sizes of the spherical flame source. Temperature – 298 K, pressure – 0.05 MPa

front appearance becomes typical for developing instability. The efficient flame velocity exceeds the predicted laminar flame velocity at 0.3 MPa.

The concentration and temperature profiles found in the simulation have allowed determination of some spherical flame peculiarities in (H_2 + CO) fuel mixture components having close combustion heat values but different reactivity and diffusion coefficients. The concentration profiles are dependent on the flame radius and the pressure (Fig. 2.34). Unlike the H_2+air system, an essential factor changing the (H_2 + CO) fuel system behavior is the fact that CO has a delayed reaction in comparison with that of H_2. The Lewis numbers for CO and H_2 are different and that leads to the peculiarities observed.

2.12 Laminar Flame Velocity in $H_2 + CH_4$ + Air Mixture

The change in the composition of $H_2 + CH_4$ fuel affects the laminar flame velocity, which is illustrated by Fig. 2.35 plotted following [76] data. It is seen that the H_2 added to CH_4 increases the laminar flame velocity, but the increase is not

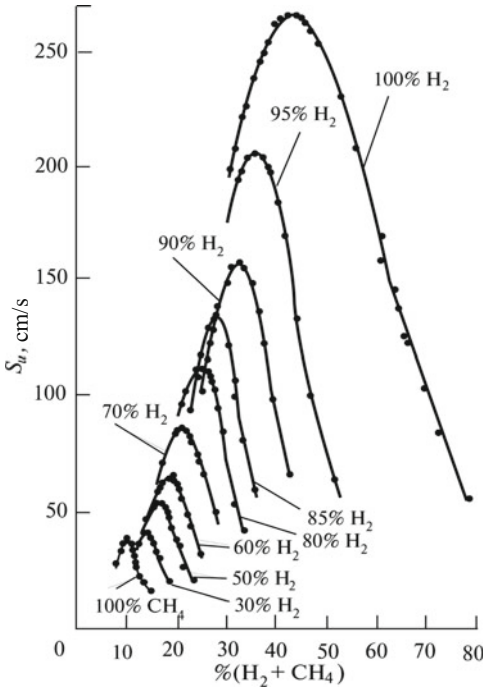

Fig. 2.35 The measured flame velocity in (H_2 + CH_4) fuel + air mixtures at the room temperature and atmospheric pressure [76]

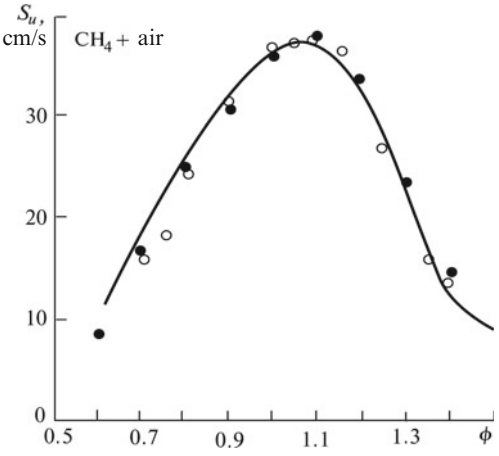

Fig. 2.36 The flame velocity in CH_4 + air mixtures at atmospheric pressure and the room temperature. The *circles* – measured results [83], the *curve* – data by the numerical simulation using the GRIMech-3 kinetic model [85]

proportional. Even a 50% H_2 content in the fuel does not greatly raise the flame velocity. Significant growth of the flame velocity is achieved in the fuel mixture with more than 90% H_2.

The data for the laminar flame velocity in a CH_4 + air mixture at atmospheric pressure and room temperature [83] are presented in Fig. 2.36 in relation to the fuel

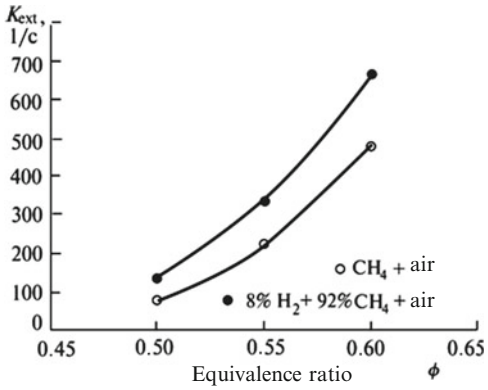

Fig. 2.37 The stretch-factor crucial for flame quenching in the near-limiting CH_4 + air mixture and in the (8% H_2 + 92% CH_4) + air mixture

excess coefficient – ϕ. The circles in the diagram show the flame velocities measured in the opposite jets burner. The open circles relate to the results measured by the laser Doppler- anemometer in [84], the solid circles correspond to the results measured by an up-dated technique using a digital image anemometer. The curve shows data obtained by numerical simulation using the GRIMech-3 kinetic model [85].

Values of the stretch-factor K_{ext} crucial for flame quenching in mixtures containing a CH_4 fuel and for CH_4 mixtures with H_2 additive have been obtained for lean near-limiting compositions [86]. Figure 2.37 shows that in an (8% H_2 + 92% CH_4) + air mixture flame quenching is more difficult (K_{ext} value is higher) than in a CH_4+air mixture. This conclusion is of practical importance because it means that an engine can run on lean mixtures.

Let us note the specific character of laminar combustion of a binary fuel H_2 + CH_4 (Hytane) in air. Assume that the volume fractions of H_2 and CH_4 are X_{H2} and X_{CH4} so that $X_{CH4} = 1 - X_{H2}$. The dependencies of the laminar flame velocity on this binary fuel composition and the fuel/air ratio are illustrated in Fig. 2.38 based on data obtained in [87, 88]. The solid curve with the solid circles correspond to experimental results, and the dashed line shows the following relations $S_{HY} = S_{H2} \cdot X_{H2} + (1 - X_{H2}) \cdot S_{CH4}$. Here S_{HY}, S_{H2} and S_{CH4} – hytane, hydrogen and methane laminar flame velocities.

It is seen that the obtained dependence is not a linear combination of known values. For $0 < X_{H2} < 0.5$ H_2 added to CH_4 has a weak effect on the flame velocity and the methane dominates the flame propagation. For hydrogen content $0.9 < X_{H2} < 1$ in the mixture, the CH_4 additive noticeably slows down the hydrogen combustion. When the binary fuel is diluted with CH_4 and in the range $0.5 < X_{H2} < 0.9$ transient variations of hydrogen combustion with moderate difficulties for flame propagation, have been observed.

An attempt was made to apply the Le Shutele law in the form

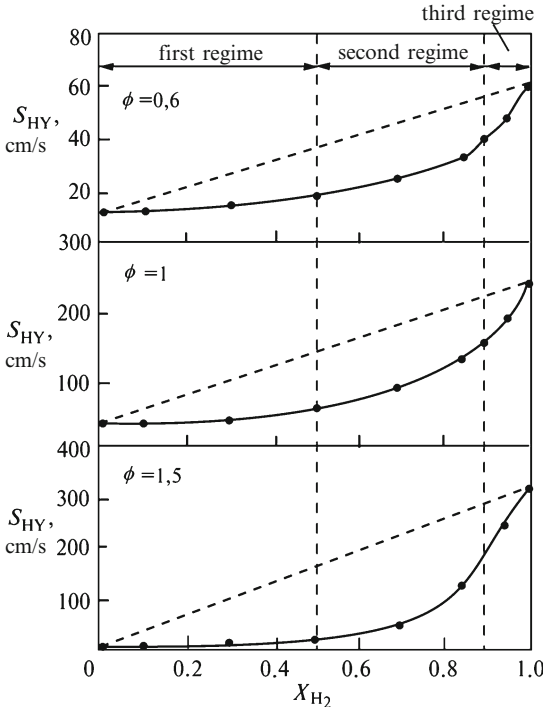

Fig. 2.38 H_2 effect on the laminar flame velocity in HYTAN + air mixture [87]: - - - - linear interpolation, ●——● experimental results

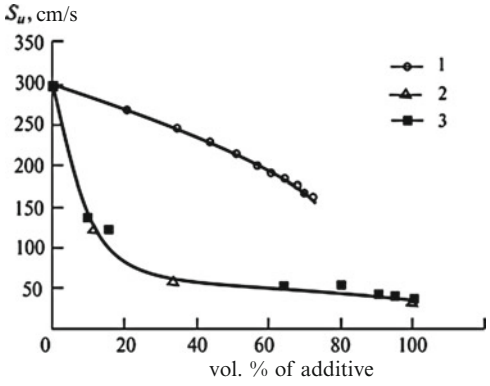

Fig. 2.39 Methane, propane and carbon dioxide effect on the laminar flame velocity of H_2 in air [89]: *1* – H_2 + CO_2; *2* – H_2 + C_3H_8; *3* – H_2 + CH_4

$$S_{HY} = \{X_{H2}/S_{H2} + (1 - X_{H2})/S_{CH4}\}^{-1}.$$

to the calculation of the binary fuel combustion velocity [87].

The investigations using the complicated models have proved the applicability of the aforementioned equation for calculations at $X_{H2} < 0.7$. At the higher content of hydrogen, the accuracy of this equation is low and it should not be used. Gaseous hydrocarbon additives can be recommended for slowing down the flame velocity in hydrogen-air mixtures. Figure 2.39 demonstrates the laminar flame velocity reduction when some of the hydrogen is replaced by carbon dioxide, methane, or propane. It is seen that the hydrocarbon additives better slow down the combustion than incombustible carbon dioxide [89].

References

1. G.E. Andrews, D. Bradley, Determination of burning velocities: a critical review. Combust. Flame **18**, 133–153 (1972)
2. G.E. Andrews, D. Bradley, Determination of burning velocity by double ignition in a closed vessel. Combust. Flame **20**, 77–89 (1973)
3. C.J. Rallis, A.M. Garforth, The determination of laminar burning velocity. Progr. Energy Combust. Sci. **6**, 303–329 (1980)
4. J.W. Linnett, Methods of measuring burning velocities. Proc. Combust. Inst. **4**, 20–35 (1953)
5. E.F. Fiock, Measurement of burning velocity, in *Physical Measurements in Gas Dynamics and Combustion*, ed. by R. Ladenburg, B. Lewis et al. (Oxford University Press, London, 1955). Chap. 11
6. L.N. Khitrin, *The physics of combustion and explosion*. Israel Program for Scientific Translations, 1962, 448 p. Jerusalem
7. A.G. Gaydon, H.G. Wolfhard, *Flames: Their Structure, Radiation and Temperature* (Chapman & Hall, London, 1979). 449 p
8. R.M. Fristrom, Definition of burning velocity and a geometric interpretation of the effects of flame curvature. Phys. Fluids **8**(2), 273–280 (1965)
9. Y.B. Zeldovich, G.I. Barenblatt, V.B. Librovich, G.M. Makhviladze, *The Mathematical Theory of Combustion and Explosions* (Consultants Bureau, New York, 1985). 597 p
10. V.A. Michelson, Uber die normale Entzundungsgeschwindigkeit Explosiver Gasgemische. Annalen der Physik und Chemie **37**, 1–24 (1889)
11. J.G. Der, *Zundvorgang in Gasgemischen* (Oldenburg, Berlin, 1934)
12. B. Lewis, G. von Elbe, *Combustion, Flames and Explosion of Gases*, 3rd edn. (Academic, Orlando, 1987). 739 p
13. Козаченко Л.С. Исследование зависимости скорости распространения пламени от физико-химических свойств топлива и аэродинамики течения газа. Диссертация. Институт химической физики АН СССР, Москва, 1954 (L.S. Kozachenko, The study of flame propagation velocity dependence on physical-chemical fuel properties and gas flow aerodynamics. Dissertation, Institute of Chemical Physics, USSR Academy of Sciences, Moscow, 1954)
14. I. Drell, F. Belles, Survey of hydrogen combustion properties. NACA Report 1383, 1958
15. E. Bartholome, Zur Metodik der Messung von Flamengeschwindigkeiten. Z. Elektrochem. **53**(4), 191–196 (1949)
16. R. Gunther, G. Janisch, Measurements of burning velocity in a flat flame front. Combust. Flame **19**, 49–53 (1972)
17. F. Takahashi, M. Mizomoto, S. Ikai, Alternative energy sources, in *Nuclear Energy. Synthetic Fuels*, ed. by T. Nejat Veziroglu, vol. 5 (New York, McGraw-Hill, 1983), p. 447
18. C.K. Wu, C.K. Law, On the determination of laminar flame speeds from stretched flames. Proc. Combust. Inst. **20**, 1941–1949 (1984)
19. D. Liu, R. MacFarlane, Laminar burning velocities of hydrogen-air flames. Combust. Flame **49**, 59–71 (1983)

20. G.W. Koroll, R.K. Kumar, E.M. Bowles, Burning velocities of hydrogen-air mixtures. Combust. Flame **94**, 330–340 (1993)
21. J. Manton, B.B. Milliken, Study of pressure dependence of burning velocity by the spherical vessel method, in *Proceedings of the Gas Dynamics Symposium (Aerothermochemistry)*, Northwestern University, Evanston, 1956, pp. 151–157
22. B. Fine, Stability limits and burning velocities of laminar hydrogen-air flames at reduced pressures. NACA TN 3833, 1956
23. S. Heimel, Effect of initial mixture temperature on burning velocity of hydrogen-air mixtures with preheating and simulated preburning. NACA TN 4156, 1957
24. J. Grumer, E.B. Cook, T.A. Kubala, Considerations pertaining to spherical-vessel combustion. Combust. Flame **3**, 437–446 (1959)
25. D.A. Senior, Burning velocities of hydrogen-air and hydrogen-oxygen mixtures. Combust. Flame **5**, 7–10 (1961)
26. T. Iijima, T. Takeno, Effects of temperature and pressure on burning velocity. Combust. Flame **65**, 35–43 (1986)
27. D.R. Dowdy, D.B. Smith, S.C. Taylor, A. Williams, The use of expanding spherical flames to determine burning velocities and stretch effects in hydrogen/air mixtures. Proc. Combust. Inst. **23**, 325–332 (1990)
28. F.N. Egolfopoulos, C.K. Law, An experimental and computational study of the burning rates of ultra-lean to moderately-rich $H_2/O_2/N_2$ laminar flames with pressure variations. Proc. Combust. Inst. **23**, 333–340 (1990)
29. C.M. Vagelopoulos, F.N. Egolfopoulos, C.K. Law, Further consideration of the determination of laminar flame speeds with the counterflow twin flame technique. Proc. Combust. Inst. **25**, 1341–1347 (1994)
30. K.T. Aung, M.I. Hassan, G.M. Faeth, Effects of pressure and nitrogen dilution on flame/stretch interactions of laminar premixed $H_2/O_2/N_2$ flames. Combust. Flame **112**, 1–16 (1998)
31. S.D. Tse, D.L. Zhu, C.K. Law, Morphology and burning rates of expanding spherical flames in H_2/O_2/inert mixtures up to 60 atmospheres. Proc. Combust. Inst. **28**, 1793–1800 (2000)
32. V.S. Babkin, Y.G. Kononenko, Equations for determining normal flame velocity in a constant-volume spherical bomb. Combust. Explos. Shock Waves **3**(2), 168–171 (1967)
33. V.S. Babkin, V.I. Babushok, Initial stage of gas combustion in a closed vessel. Combust. Explos. Shock Waves **13**(1), 19–23 (1977)
34. H. Behrens, Flame instabilities and combustion mechanism. Proc. Combust. Inst. **4**, 538–545 (1953)
35. I.E. Garside, B. Jackson, The formation and some properties of polyhedral burner flames. Proc. Combust. Inst. **4**, 545–552 (1953)
36. C.K. Law, S. Ishizuka, P. Cho, On the opening of premixed bunsen flame tips. Combust. Sci. Technol. **28**, 89–96 (1982)
37. J.D.A. Buckmaster, Mathematical description of open and closed flame tips. Combust. Sci. Technol. **20**, 33–40 (1979)
38. G. Dixon-Lewis, Spherically symmetric flame propagation in hydrogen-air mixtures. Combust. Sci. Technol. **34**, 1–29 (1983)
39. A.M. Garforth, C.J. Rallis, The spherical bomb method for laminar burning velocity determination: equipment, experimental procedure and data handling. Report No. 65, University of the Witwatersrand, Johannesburg, 1976
40. D. Bradley, A. Mitcheson, Mathematical solution for explosions in spherical vessels. Combust. Flame **26**, 201–217 (1976)
41. B.E. Milton, J.C. Keck, Laminar burning velocities in stoichiometric hydrogen and hydrogen-hydrocarbon gas mixtures. Combust. Flame **58**, 13–22 (1984)
42. O.C. Kwon, G. Rozenchan, C.K. Law, Cellular instabilities and self-acceleration of outwardly propagating spherical flames. Proc. Combust. Inst. **29**, 1775–1783 (2002)
43. C.J. Sun, C.J. Sung, L. He, C.K. Law, Dynamics of weakly stretched flames: quantitative description and extraction of global flame parameters. Combust. Flame **118**, 108–128 (1999)

44. G.W. Koroll, S.R. Mulpuru, The effect of dilution with steam on the burning velocity and structure of premixed hydrogen flames. Proc. Combust. Inst. **21**, 1811–1819 (1986)
45. S.M. Kogarko, A.G. Lyamin, O.E. Popov, A.Y. Kusharin, A.V. Dubrovin, Determination of flame propagation limits in stoichiometric oxyhydrogen mixtures with steam. In: *Hydrogen Behaviour and Control and Related Containment Loading Aspects*. IAEA-TC-476.6, Vienna, 1984, pp. 37–41
46. B.W. Marshall Jr., Hydrogen-air-steam flammability limits and combustion characteristics in the FITS vessel. NUREG/CR-3468, SAND84-0383, 1986
47. J.K. Worrell, S.C. Taylor, C. Robinson, D.B. Smith, The use of detailed computer modeling to test burning velocity and Markstein length measurement using expanding spherical flames, in *Proceedings of the Anglo-German Combustion Symposium*, Cambridge, UK, 1993, pp. 364–367
48. M.J. Brown, I.C. McLean, D.B. Smith, S.C. Taylor, Markstein lengths of CO/H_2/air flames, using expanding spherical flames. Proc. Combust. Inst. **26**, 875–881 (1996)
49. O.C. Kwon, G.M. Faeth, Flame/stretch interactions of premixed hydrogen-fueled flames: measurements and predictions. Combust. Flame **124**, 590–610 (2001)
50. K.T. Aung, M.I. Hassan, G.M. Faeth, Flame stretch interactions of laminar premixed hydrogen/air flames at normal temperature and pressure. Combust. Flame **109**, 1–24 (1997)
51. Попов О.Е. Ламинарная скорость горения в сферическом газовом пламени. Химическая физика процессов горения и взрыва, 12 Симпозиум по горению и взрыву. Черноголовка, 2000, ч.1. С. 128–129 (O.E. Popov, Laminar burning velocity in spherical gas flame. Khimicheskaya Fizika Processov Gorenia i Vzryva. Chernogolovka, 2000, part 1, pp. 128–129)
52. L.-K. Tseng, M.A. Ismail, G.M. Faeth, Laminar burning velocities and Markstein numbers of hydrocarbon/air flames. Combust. Flame **95**, 410–426 (1993)
53. G.W. Koroll, R.K. Kumar, C.K. Chan, Combustion behaviour in the moderator cover gas, in *Proceedings of the 9th Annual Canadian Nuclear Society Conference*, Winnipeg, 1988, pp. 238–244
54. F. Behrendt, J. Warnatz, The dependence of flame propagation in H_2-O_2-N_2 mixtures on temperature, pressure and initial composition. Int. J. Hydrogen Energy **10**, 749–755 (1985)
55. F. Mauss, N. Peters, B. Rogg, F.A. Williams, Reduced kinetic mechanisms for premixed hydrogen flames, in *Reduced Kinetic Mechanisms for Applications in Combustion Systems*, ed. by N. Peters, B. Rogg. Lecture notes in physics, vol. 15 (Springer, Heidelberg, 1993), p. 29
56. G. Dixon-Lewis, Kinetic mechanism, structure and properties of premixed flames in hydrogen-oxygen-nitrogen mixtures. Phil. Trans. R. Soc. London **A292**(1388), 45–99 (1979)
57. M.D. Smooke, J.A. Miller, R.J. Kee, Determination of adiabatic flame speeds by boundary value methods. Combust. Sci. Technol. **34**, 79–90 (1983)
58. R.J. Kee, J.F. Grcar, M.D. Smooke, J.A. Miller, A Fortran program for modeling steady laminar one-dimensional flames. Sandia Report SAND85-8240, 1985
59. D.B. Spalding, The theory of flow phenomena with a chain reaction. Phil. Trans. R. Soc. London **A249**, 1–25 (1956)
60. Кушарин А.Ю., Попов О.Е., Агафонов Г.Л. Нормальные скорости пламени в смесях гремучего газа с водяным паром. Химическая физика, 1995. Т. 14, № 4. С. 179–189 (A.Y. Kusharin, O.E. Popov, G.L. Agafonov, Normal flame velocities in mixtures of oxyhydrogen gas with water steam. Himicheskaya Fizika **14**(4), 179–189 (1995))
61. R.A. Yetter, F.L. Dryer, H. Rabitz, A comprehensive reaction mechanism for carbon monoxide/hydrogen/oxygen kinetics. Combust. Sci. Technol. **79**, 97–128 (1991)
62. R.J. Kee, G. Dixon-Lewis, J. Warnatz, M.E. Coltrin, J.A. Miller, A FORTRAN computer code package for the evaluation of gas-phase, multicomponent transport properties. Sandia Report SAND86-8246, 1986
63. N.M. Marinov, C.K. Westbrook, W.J. Pitz, *Detailed and Global Chemical Kinetics Model for Hydrogen*. Lawrence Livermore National Laboratory, Preprint UCRL-JC-120677, 1995

64. D.L. Baulch, C.J. Cobos, R.A. Cox, C. Esser, P. Frank, Th Just, J.A. Kerr, M.J. Pilling, J. Troe, R.W. Walker, J. Warnatz, Evaluated kinetic data for combustion modelling. J. Phys. Chem. Ref. Data **21**(3), 411–736 (1992)
65. D.L. Baulch, C.J. Cobos, R.A. Cox, P. Frank, G. Hayman, Th Just, J.A. Kerr, T. Murrels, M.J. Pilling, J. Troe, R.W. Walker, J. Warnatz, Summary table of evaluated kinetic data for combustion modeling: supplement I. Combust. Flame **98**, 59–79 (1994)
66. R. Edse, L.R. Lawrence, Detonation induction phenomena and flame propagation rates in low temperature hydrogen-oxygen mixtures. Combust. Flame **13**, 479–486 (1969)
67. B. Lewis, *AGARD Selected Combustion Problems: Fundamentals and Aeronautical Applications* (Butterworths Science, London, 1954), pp. 176–179
68. R.A. Strehlow, *Fundamentals of Combustion* (Int. Textbook Company, Scranton, 1968)
69. Y.N. Shebeko, S.G. Tsarichenko, A.Y. Korolchenko, A.V. Trunev, V.Y. Navzenya, S.N. Papkov, A.A. Zaitzev, Burning velocities and flammability limits of gaseous mixtures at elevated temperatures and pressures. Combust. Flame **102**, 427–437 (1995)
70. B.E. Gelfand, O.E. Popov, V.P. Karpov, A.Y. Kusharin, G.L. Agafonov, Laminar and turbulent flame propagation in hydrogen-air-steam mixtures at accident relevant pressure-temperature conditions. Report IChPh-INR, 1995
71. V.S. Babkin, A.V. V'yun, Inhibition of hydrogen-air flame at high pressures. Combust. Explos. Shock Waves **17**(5), 483–488 (1981)
72. J.T. Agnew, L.B. Graiff, The pressure dependence of laminar burning velocity by the spherical bomb method. Combust. Flame **5**, 209–219 (1961)
73. A.Y. Kusharin, O.E. Popov, G.L. Agafonov, Burning velocities of oxygen-hydrogen mixtures with steam. Chem. Phys. Rep. **14**(4), 584–594 (1995)
74. M. Kuznetsov, J. Grune, R. Redlinger, W. Breitung, N. Ichikawa, Laminar burning velocities of hydrogen-oxygen-steam mixtures at various temperatures and pressures, in *Proceedings of 3rd European Combustion Meeting*, ECM 2007, Chania
75. Y.N. Shebeko, A.Y. Korol'chenko, S.G. Tsarichenko, V.Y. Navtsenya, V.L. Malkin, Effects of the initial prssure and temperature on the combustion characteristics of hydrogen-containing mixtures. Combust. Explos. Shock Waves **25**(3), 289–292 (1989)
76. T.G. Sholte, P.B. Vaags, Burning velocities of mixtures of hydrogen, carbon monoxide and methane with air. Combust. Flame **3**, 511–524 (1959)
77. I.C. McLean, D.B. Smith, S.C. Taylor, The use of carbon monoxide/hydrogen burning velocities to examine the rate of the CO+OH reaction. Proc. Combust. Inst. **25**, 749–757 (1994)
78. A.A. Konnov, Detailed reaction mechanism for small hydrocarbons combustion, 2007, http: // homepages.vub.ac.be/~akonnov/
79. M.I. Hassan, K.T. Aung, G.M. Faeth, Properties of laminar premixed CO/H_2/air flames at various pressures. J. Propul. Power **13**, 239–245 (1997)
80. Карпов В.П., Кушарин А.Ю., Попов О.Е., Гельфанд Б.Е. Экспериментальные наблюдения и численное моделирование горения в бедных смесях H_2-CO-воздух в сферической бомбе. Химическая физика процессов горения и взрыва, 12 Симпозиум по горению и взрыву. Черноголовка, 2000, ч.1. С. 72–74 (V.P. Karpov, A.Y. Kusharin, O.E. Popov, B.E. Gelfand, Experimental observations and numerical simulation of burning in lean H_2-CO-air mixtures in spherical bomb. Khimicheskaya Fizika Processov Gorenia i Vzryva. Chernogolovka, 2000, part 1, pp. 72–74)
81. O.E. Popov, V.P. Karpov, B.E. Gelfand, S.V. Khomik, Combustion and explosion characteristics of H_2-CO-air mixtures, in *Proceedings of Third Asia-Pacific Conference on Combustion*, Seoul, 2001, pp. 730–733
82. B.E. Gelfand, V.P. Karpov, O.E. Popov, Turbulent flames in lean H_2-air-CO_2 mixtures, in *Proceedings of First Mediterranean Symposium on Combustion*, Antalya, 1999, pp. 1000–1006

83. Y. Dong, C.M. Vagelopoulos, G.R. Spedding, F.N. Egolfopoulos, Measurement of laminar flame speeds through digital particle image velocimetry: mixtures of methane and ethane with hydrogen, oxygen, nitrogen, and helium. Proc. Combust. Inst. **29**, 1419–1426 (2002)
84. C.M. Vagelopoulos, F.N. Egolfopoulos, Laminar flame speeds and extinction strain rates of mixtures of carbon monoxide with hydrogen, methane and air. Proc. Combust. Inst. **25**, 1317–1323 (1994)
85. C.T. Bowman, M. Frenklach, W.R. Gardiner, G. Smith, The GRI 3.0 chemical kinetic mechanism, 1999, http://www.me.berkeley.edu/grimech/
86. J.Y. Ren, W. Qin, F.N. Egolfopoulos, T.T. Tsotsis, Strain-rate effects on hydrogen-enhanced lean premixed combustion. Combust. Flame **124**, 717–720 (2001)
87. V. Di Sarli, A. Di Benedetto, Laminar burning velocity of hydrogen-air premixed flames. Int. J. Hydrog. Energy **32**, 637–646 (2007)
88. K.S. Raman, Laminar burning velocities of lean H_2+air mixtures. EDL report FM97-15, CalTech, 1997
89. Y. Wu, Y. Lu, I.S. Al-rachbi, G.T. Kalghati, Prediction of the liftoff, blowout and blowoff stability limits of pure hydrogen and hydrogen/hydrocarbon mixture jet flames. International Conference on Hydrogen Safety, San Sebastian, Spain, 2007

http://www.springer.com/978-3-642-25351-5

Thermo-Gas Dynamics of Hydrogen Combustion and Explosion

Gelfand, B.E.; Silnikov, M.V.; Medvedev, S.P.; Khomik, S.V.

2012, XXII, 326 p., Hardcover
ISBN: 978-3-642-25351-5